https://doi.org/10.15255/KUI.2024.024
KUI-41/2024
Original scientific paper
Received June 28, 2024
Accepted September 2, 2024

Chitosan/Bioactive Glass Scaffolds as Potential Drug Carriers

L. Dornjak,* and *A. Rogina*
University of Zagreb Faculty of Chemical Engineering and Technology, Trg Marka Marulića 19, 10 000 Zagreb, Croatia

Abstract

Modern chemotherapeutic agents offer versatile and potent applications for treatment of various forms of sarcomas. One such agent, doxorubicin, offers potent chemotherapeutic effects through its property of intercalation with DNA, resulting in rapid DNA degradation and cancer cell apoptosis. Despite its advanced properties, its application causes system-wide damage leading to cardiotoxicity and even lowering of cognitive scores, inhibition of self-regeneration, and nephropathy. To circumvent these adverse side-effects, localised drug delivery via a polymeric composite material may offer a solution. Chitosan, a biodegradable polymer, is a biocompatible polysaccharide capable of acting as an effective polymeric matrix for targeted drug delivery. In combination with bioactive glass, a composite polymeric scaffold could enhance the incorporation and release kinetics of doxorubicin from the polymer-based carrier while also promoting the formation of regenerative bone-like apatite.

This work aimed to prepare chitosan/bioactive glass composite scaffolds as biodegradable carriers for doxorubicin in bone tumour treatment. The composite scaffolds were prepared with varying weight fractions of bioactive glass (0–30 %) within the chitosan matrix using thermally induced phase separation followed by solvent sublimation. The resulting scaffolds were characterised using X-ray diffraction, Fourier transform infrared spectroscopy, and scanning electron microscopy assisted with energy-dispersive X-ray spectroscopy. The drug was loaded into the scaffolds by immersing them in doxorubicin solutions of different concentrations (25 and 50 ppm) for 5 h. The release of doxorubicin was then studied in a phosphate buffer solution (pH 7.4) over a 24-h period using fluorescence spectrometry after scaffold immersion.

Keywords

Chitosan, polymer, bioactive glass, doxorubicin, osteosarcoma, composite

1 Introduction

Cancer remains a significant challenge in modern medicine when it comes to research and innovation. Chemotherapy is a mainstay and a widely used form of treatment in combating various cancers.[1,2] However, despite its proven effectiveness, chemotherapy is accompanied by systemic side-effects, including systemic toxicity, non-specificity, and multidrug resistance.[3] One such chemotherapeutic agent is doxorubicin (DOX), part of the anthracycline antibiotic group of chemotherapeutic agents widely used for their potent efficacy against a broad spectrum of cancers, such as breast cancer, lymphomas, and osteosarcomas.[4,5] Its efficacy arises from its mechanism of action, involving intercalation with DNA double helix strands, and/or through covalent bonding to proteins associated with DNA replication and transcription, resulting in the inhibition of the enzyme topoisomerase II, preventing the replication of rapidly dividing cancer cells, thereby inducing cancer cell apoptosis.[6,7] Despite its effectiveness, doxorubicin can cause severe side effects, including permanent damage to the heart, brain, liver, and kidneys, potentially leading to impaired organ health or nephropathy[8–11]. These side effects primarily stem from the generation of free radicals as a consequence of treatment.[12,13] As a result, there is a critical compromise between treating cancer and avoiding long-term harm to the patient's health.

Such limitations necessitate the development of more advanced drug delivery systems, which would allow for targeted drug delivery, thereby enhancing therapeutic efficacy while minimising adverse effects. Modern approaches in drug delivery include liposomes,[14] polymeric materials,[15,16] metals[17,18] and bioceramics.[19] Beyond targeted drug release, these systems should also promote simultaneous healing and regeneration of damaged tissue during treatment. This dual functionality makes such delivery systems especially promising for therapies requiring both effective drug delivery and tissue repair. Such modifications are made through interfacing with materials such as: bone-forming bioceramics,[20] growth factors,[21] proteins,[22] ions,[23] *etc.*

* Corresponding author: Luka Dornjak, mag. chem.
e-mail: ldornjak@fkit.unizg.hr

A widely used preparation method for such materials includes the entrapment of DOX in positively charged carriers, which would favour cell adhesion and cellular uptake due to their attraction to negatively charged cell membranes.[24] A common category of materials used for formulating these carriers are natural polymeric systems. Among these, chitosan, a natural linear polymer, stands out as a preferred carrier due to its favourable properties. Its polycationic structure confers unique characteristics such as mucoadhesiveness, pH sensitivity, and antibacterial activity, while also enabling interactions with various biomolecules (e.g., DNA, lipids, proteins).[25,26] Additionally, its hydrogel nature makes it a viable polymeric matrix for encapsulating biomolecules, drugs, ions, and other modifications, while also mimicking the extracellular matrix (ECM) for a less disruptive application during treatment.[27]

Despite its many advantages, chitosan alone falls short when it comes to bone tissue interaction and regeneration. These limitations are imposed due to the lack of osteoinductive and osteoconductive properties required to encourage proliferation and differentiation of progenitor cells such as mesenchymal stem cells (MSC), into bone cells.[28] To overcome these deficiencies, chitosan can be combined with bioactive glass (BG), creating a composite material that significantly enhances its utility in bone tissue engineering. According to Sergi et al.,[29] bioactive glass has the ability to form an interactive hydroxyapatite (HAp) layer on the material surface when in contact with biological fluids. Since HAp is a building block of natural human bone,[30] along with organic-inorganic materials such as collagen, fibrils and nano-crystallites,[31] the presence of the apatite layer results in the creation of a class A bioactive index biomaterial possessing both osteoconductive and osteoproductive properties.[32] These next-generation biomaterials represent the ideal combination of bioactivity and natural polymer properties, which closely mimic natural bone function and activities like in-vivo bone regeneration mechanisms.

In this study, we propose a chitosan/bioactive glass composite scaffold as a potential delivery system for DOX to locally treat residual bone tumour cells after surgical resection. The addition of BG to the chitosan polymer matrix allows for the promotion of osteoinductive and osteoconductive properties by forming an interactive apatite layer on the surface of the composite.

Furthermore, we examined the influence of varying bioactive glass content on the drug release of the composite scaffolds.

The CHT/BG scaffolds were prepared through thermally induced phase separation (TIPS) followed by solvent sublimation. DOX was encapsulated through adsorption by immersing the scaffolds in a DOX solution, while preserving their porous 3D interconnected structure. The drug release profile of the composite scaffolds showed no significant changes with increased BG content. The chitosan/BG composite scaffolds were designed as a possible structure in aiding localised bone tumour treatment with enhanced osteoinductive and osteoconductive behaviour.

2 Experimental

2.1 Materials

Tetraethyl orthosilicate (TEOS) 99 %+ BDH Prolabo, nitric acid (HNO_3) 65 % POCH, tris(hydroxymethyl)aminomethane (TRIS), di-potassium hydrogen orthophosphate trihydrate ($K_2HPO_4{\cdot}3H_2O$), and ammonia (NH_3) were acquired from VWR (Radnor, Pennsylvania, USA). Triethyl phosphate (TEP) was obtained from Sigma-Aldrich (St. Louis, Missouri, USA), calcium nitrate (CaCO3) from Kemika (Zagreb, Croatia), and chitosan (CHT) with a degree of deacetylation (DD) of 83 % and viscosity of 293 mPa was purchased from Heppe (Germany). Acetic acid was purchased from Lachner (Neratovice, Czech Republic), and acetone (p.a.) from T.T.T (Sveta Nedelja, Croatia). Sodium sulphate anhydrous (Na_2SO_4), potassium chloride (KCl), magnesium chloride hexahydrate ($MgCl_2{\cdot}6H_2O$) and sodium hydrogen carbonate ($NaHCO_3$) were purchased from Gram-Mol (Zagreb, Croatia). Calcium chloride ($CaCl_2$) was obtained from Thermo Fisher Scientific (Waltham, Massachusetts, United States).

2.2 Synthesis of bioactive glass

A rapid alkali-mediated sol-gel synthesis route, based on the method described by Moonesi et al.,[33] was used to synthesise the bioactive glass. Firstly, TEOS was mixed with 2 mol dm^{-3} nitric acid and deionised water to undergo acid hydrolysis for 1 h. Following this, TEP was added, and the solution was stirred for 20 min. Next, $Ca(NO_3)_2$ was added to the clear sol, and NH_3 was introduced dropwise until gelation occurred. The resulting gel was dried at 60 °C for 24 h and subjected to thermal treatment at 600 °C for 2 h in a muffle furnace.

2.3 Preparation of composite scaffolds

Chitosan was dissolved in a 0.5 % (v/v) acetic acid solution and stirred for 4 h to obtain a 1.2 % (w/v) chitosan solution. An appropriate amount of bioactive glass was added to the chitosan solution to obtain a CHT/BG suspension (wt. = 0, 10, 20, 30 %). The suspension was then stirred for 24 h to ensure homogenisation. The resulting solutions were cast

into 24-well plates and frozen at –22 °C for 24 h. The frozen samples were then lyophilised for 48 h using a Kambic LIO-5PLT freeze dryer. The dry scaffolds were then immersed in a 0.5 mol dm^{-3} NaOH solution to neutralise any residual acetic acid, and subsequently washed with deionised water until a neutral pH was reached. The samples were labelled as BG0, BG10, BG20, and BG30 corresponding to the increasing weight fraction of BG.

2.4 Composite scaffold identification

The scaffolds were analysed using Fourier transform infrared spectroscopy (ATR-FTIR) with a Bruker Vertex spectrometer at a resolution of 2 cm^{-1} and a spectral range of 4000–400 cm^{-1} with 32 scans at 20 °C.

The mineralogical composition was determined by X-ray diffraction analysis (XRD) on a Shimadzu XRD 6000 instrument using CuKα radiation at 30 kV and 30 mA. The X-ray patterns were recorded in step mode, covering 2θ angles from 5° to 60°, with a step size of 0.02° and a step hold time of 0.6 s. The microstructure of the composite scaffolds was imaged using a TESCAN Vega3 SEM Easyprobe scanning electron microscope (SEM) with an electron beam energy of 10 keV. Elemental composition was determined using an energy-dispersive X-ray (EDS) spectrometer connected to the electron microscope. Before SEM/EDS analysis, the composite samples were sputter-coated with gold and palladium.

2.5 *In vitro* bioactivity study

In vitro bioactivity was assessed by immersing a circular composite scaffold sample (≈10×1 mm ($d \times h$)) in 20 ml of simulated body fluid (SBF) for 21 days at 37 °C. The SBF medium was previously prepared in Milli-Q water, buffered with Tris and HCl to a pH of 7.4, following the protocol described by *Kokubo et al.*[34] The SBF medium was refreshed every two days to maintain proper ionic saturation. After 21 days, the samples were removed from the SBF, carefully rinsed with deionised water to remove residual salts, frozen, and lyophilised to ensure they were fully dried.

2.6 *In vitro* drug release study

The composite scaffolds were loaded with DOX as follows: chitosan/BG scaffolds were prepared as previously outlined. Subsequently, different concentrations of DOX solution (25 and 50 ppm) were added to the scaffold-containing wells, and left for 5 h in light-deprived conditions. The scaffolds were once again frozen and lyophilised. The resulting DOX-loaded scaffolds were labelled as BG0-DOX25, BG0-DOX 50, BG10-DOX25, BG10-DOX50, BG20-DOX25, BG20-DOX50, BG30-DOX25, BG30-DOX50, corresponding to the concentration of the DOX loading solution.

The release of DOX was evaluated in phosphate buffer (PB, pH 7.4) over 24 h at 37 °C. At predetermined intervals (time points 1, 3, 6, 12, and 24 h), supernatant samples were collected and analysed using fluorescence spectrometry.

Fluorescence analysis was conducted using a PerkinElmer Victor Nivo Multimode Microplate Reader HH3500 with an excitation filter set at 480/30 nm and an emission filter set at 530/30 nm. Quantification was performed within the calibration range of 0.5–10 ppm. All measurements were carried out in triplicate. The obtained values are reported as the mean ± standard deviation (SD) of the three individual samples.

2.7 Statistics

The results are presented as mean values ± standard deviation. Data differences were evaluated using a two-way analysis of variance (ANOVA), followed by a Tukey post hoc test. Significant differences between groups are denoted with an asterisk (*).

3 Results and discussion

3.1 FTIR analysis

The obtained composites were identified using ATR-FTIR spectroscopy. As shown in Fig. 1A, the chitosan scaffolds exhibited distinct absorption bands. The region between 3400 and 3300 cm^{-1} shows overlapping bands that correspond to the stretching vibrations of hydroxyl and amino groups, along with their interactions through hydrogen bonds.[35] Two absorption bands at 2926 and 2868 cm^{-1}, are attributed to the symmetric and asymmetric stretching of C–H bonds in the $–CH_2$ functional group.[36] Additionally, the two absorption bands at 1651, 1583, and 1553 cm^{-1} are assigned to amide I (C=O), amino ($–NH_2$) and amide II (–NH) respectively.[37] The three distinct absorption bands at 1417, 1376, and 1322 cm^{-1} can be associated with the bending mode of $–CH_2$ in the pyranose ring and $–CH_3$ groups, combined with the stretching vibrations of the C–N bond (amide III).[38,39] Finally, the absorption bands at 1150, 1059, and 1025 cm^{-1} correspond to the stretching vibrations of the C–O bond in the glucosamine unit.[40]

The FTIR spectrum of the prepared bioactive glass (Fig. 1B) showed several distinct absorption bands. The small, broadening absorption band at 1220 cm^{-1} may be

attributed to the possible adsorption of CO_2. The absorption band between 1100–950 cm^{-1} is associated with the asymmetric stretching of Si–O–Si.[33] Further, a weak absorption band at 925 cm^{-1} is likely related to Si–O–Ca or non-bridging oxygen (NBO).[41,42] Lastly, the absorption peak observed at 459 cm^{-1} corresponds to the Si–O–Si stretching vibration.[43] The FTIR spectrum of the composite scaffolds shows the superposition of the chitosan and bioactive glass spectra. Subtle changes in the spectrum were observed with the incorporation of BG into the polymer matrix. The composite spectra show a broadening of the absorption band related to C–O–C, along with the appearance of phosphate absorption bands at 602 and 561 cm^{-1}, and a shift in the stretching vibration of Si–O–Si[43,44] indicating the presence of BG within the chitosan matrix.

3.2 XRD analysis

The XRD analysis of the composite scaffolds is presented in Fig. 1C. The broad diffraction maximum at $2\theta \approx 21.3°$ can be attributed to the primary diffraction maximum of chitosan. The addition of BG into the polymeric matrix resulted in a small diffraction maximum at $2\theta \approx 31.72°$, corresponding to the diffraction maxima of calcium silicate from BG. The XRD pattern of the prepared bioactive glass is shown in Fig. 1D. The obtained BG exhibited a diffraction maximum at $2\theta = 31.75°$ followed by a weak diffraction maximum at $2\theta = 39.7°$, 46.8° and 49.5°. The highest diffraction maxima can be attributed to the orthorhombic belite polymorph of dicalcium silicates (Ca_2SiO_4), as referenced by the ICDD data (ICDD 29-0369), as shown in Fig. 1E. The presence of weak diffraction maxima weak at $2\theta = 39.7°$, 46.8° and 49.5°, may indicate the formation of hydroxyapatite during synthesis, as shown in Fig. 3F. The broad diffraction maximum indicates an amorphous structure of the bioactive glass, accompanied by the sharp diffraction maximum of belite. According to *Pirayesh et al.*[45], crystalline bioactive materials tend to exhibit reduced bioactive properties compared to amorphous structures of the same composition due to their more thermodynamically more stable structures. This increase in stability, caused by the more crystalline form, reduces their reactivity and subsequent interactions with a biological environment. In contrast, amorphous materials, with their higher energy state and greater surface area, exhibit enhanced reactivity, leading to improved bioactivity. As such, the use of amorphous materials in biomedicine can be a more advantageous approach for promoting desired biological responses and integration with host tissue.

3.3 Scaffold microstructure and elemental analysis

The microstructure of the composite scaffolds exhibited high porosity and an interconnected, irregular structure, as illustrated in Fig. 2. As previously mentioned, the samples were prepared using the TIPS method followed by lyophilisation. The resulting porous structures contained irregular, interconnected pores with pore size ranging from 100–200 μm, as observed in SEM micrographs (Fig. 2A).

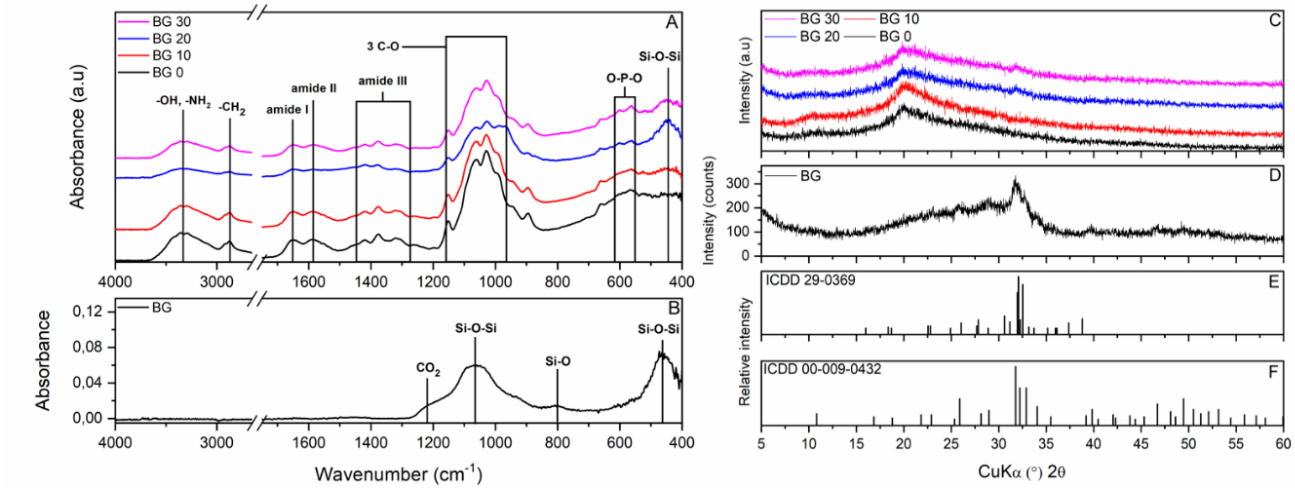

Fig. 1 – FTIR spectra of (A) chitosan and composite scaffolds, (B) pure bioactive glass; XRD pattern of (C) chitosan and composite scaffolds, (D) obtained bioactive glass; (E) ICDD calcium silicate standard data, and (F) ICDD hydroxyapatite standard data

Slika 1 – FTIR spektri (A) kitozana i kompozitnih okosnica, (B) čistog bioaktivnog stakla; XRD difraktogram (C) kitozana i kompozitnih okosnica, (D) dobivenog bioaktivnog stakla; (E) ICDD standard kalcijeva silikata i (F) ICDD standard hidroksiapatita

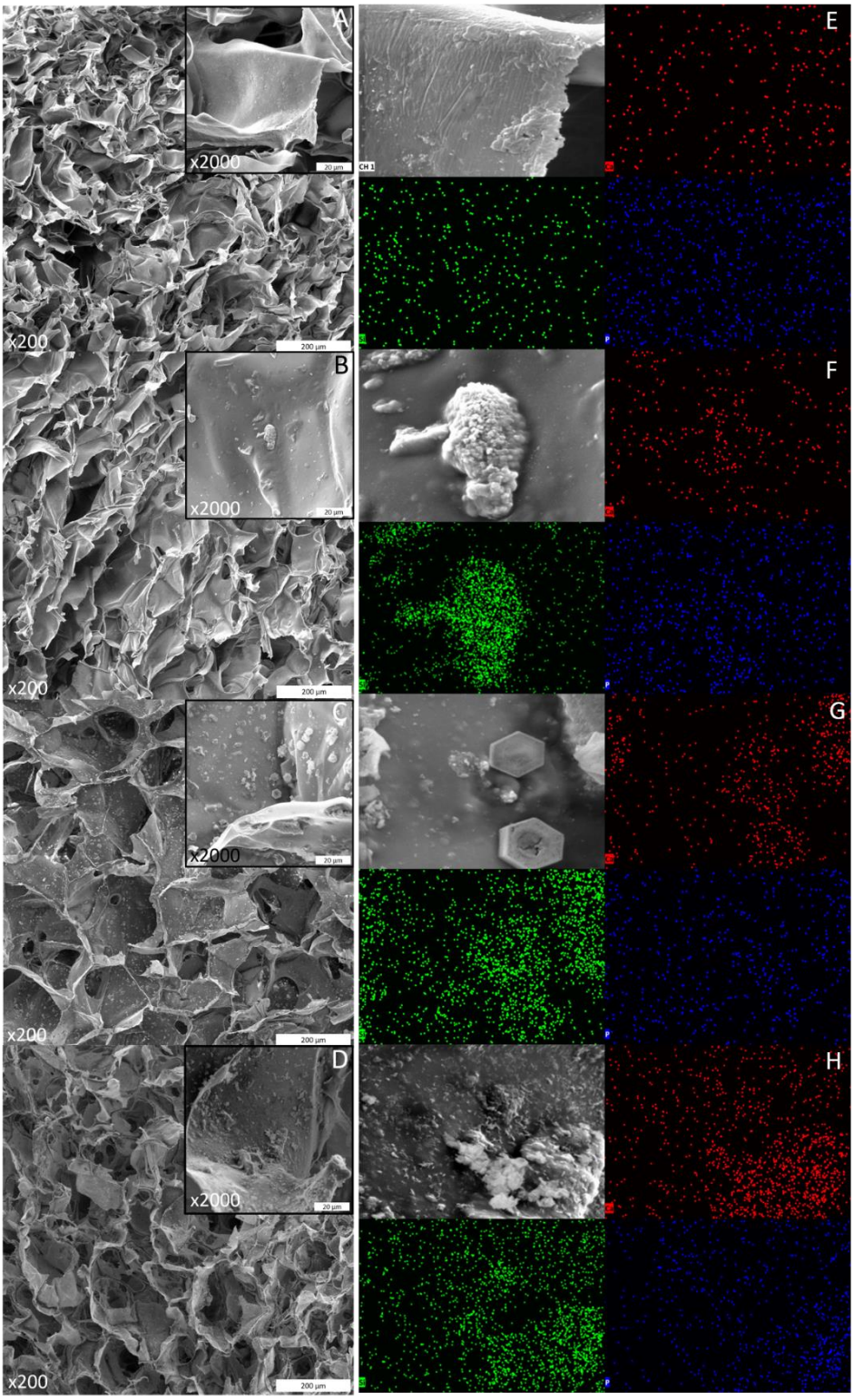

Fig. 2 – SEM micrographs of (A) BG0, (B) BG10, (C) BG20, and (D) BG30 scaffold. The scale bar on SEM micrographs: 200 µm and 20 µm; EDS mapping of (E) BG0, (F) BG10, (G) BG20, and (H) BG30 scaffold indicating the distribution of calcium (red), silicon (green), and phosphorus (blue)

Slika 2 – SEM mikrografije (A) BG0, (B) BG10, (C) BG20 i (D) BG30 okosnica. Mjerna skala na SEM mikrografijama: 200 µm i 20 µm; EDS mapiranje elemenata na (E) BG0, (F) BG10, (G) BG20 i (H) BG30 okosnicama: kalcij (crveno), silicij (zeleno) i fosfor (plavo)

The addition of BG into the polymeric matrix resulted in no significant changes in the microstructure of the obtained composite scaffolds; the pore shape remained irregular, and the pore size reached up to 300 μm (Figs. 2B–2D). Moreover, the interconnectivity of the pores was maintained. Drastic changes in terms of individual particles and agglomerates were observed on the pore surfaces, especially with a greater amount of BG. Some of these agglomerates were highly exposed on the polymer surface, which could enhance the bioactivity of the scaffold.

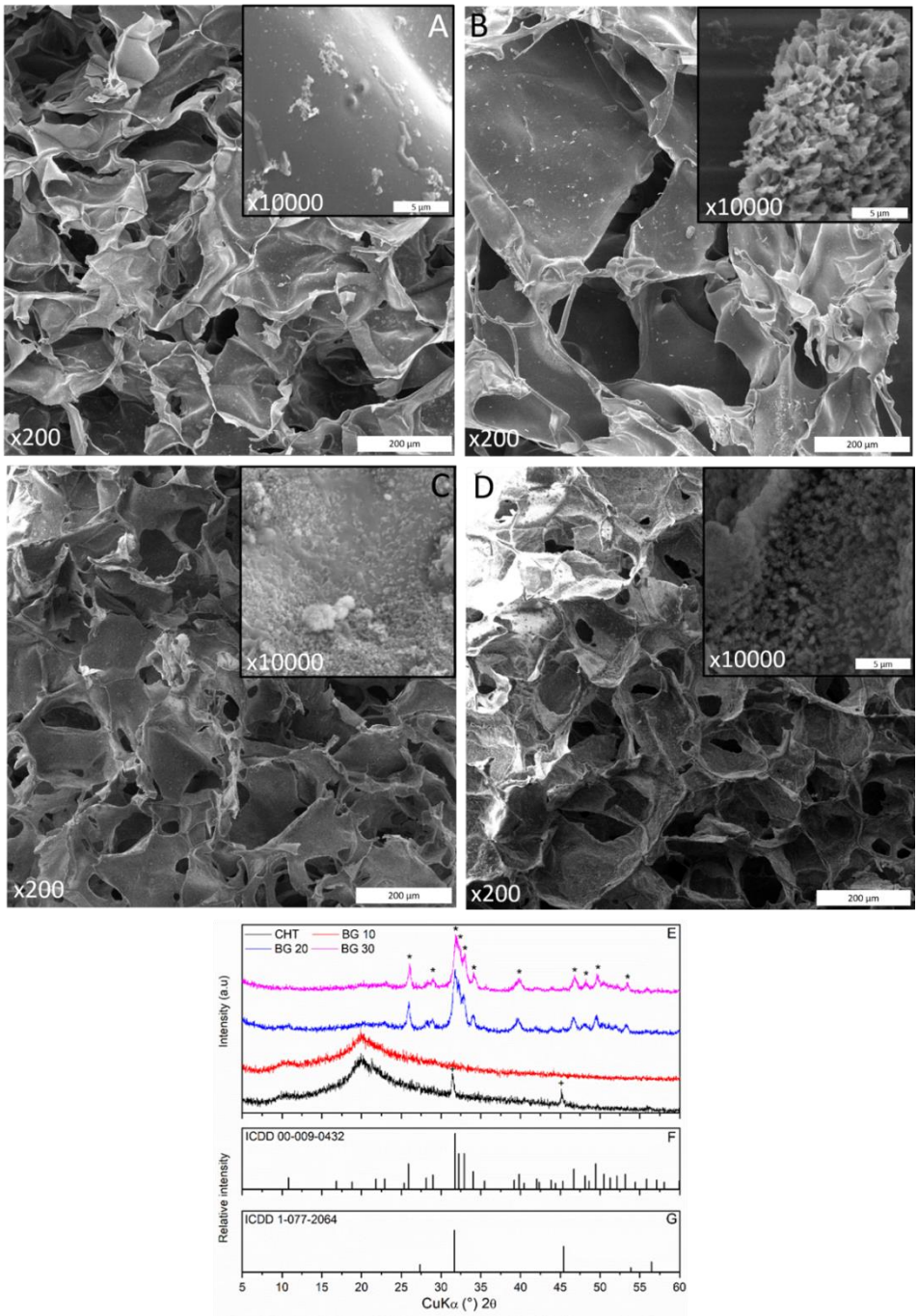

Fig. 3 – SEM micrographs of the surface of (A) BG0; (B) BG10; (C) BG20, and (D) BG30 scaffold after incubation in SBF for 21 days; XRD patterns of (E) composite scaffolds after 21 days of SBF incubation, (F) ICDD hydroxyapatite standard data, and (G) ICDD sodium chloride standard data ('*' hydroxyapatite, '$^{+}$' sodium chloride)

Slika 3 – SEM mikrofotografije površine (A) BG0; (B) BG10; (C) BG20 i (D) BG30 okosnica nakon 21 dana inkubacije u SBF otopini; XRD difraktogram (E) kompozitnih okosnica, (F) ICDD standard hidroksiapatita i (G) ICDD standard natrijeva klorida ('*' hidroksiapatit, '$^{+}$' natrijev klorid)

A porous structure is a crucial attribute for cellular uptake for several reasons. Firstly, the structure facilitates efficient diffusion of nutrients such as oxygen, and the removal of waste products, essential for maintaining cell viability and promoting cell health.[46] Secondly, the porous structure mimics the natural extracellular matrix, creating an optimal environment for cell adhesion, proliferation, and differentiation.[47] Furthermore, the scaffold's porous structure influences drug release, offering a controlled and sustained delivery mechanism. The interconnected nature of the porous structure provides an extensive surface area, facilitating efficient drug loading and subsequent release. Tailoring the scaffold's morphology allows for modulation of the release profile of the encapsulated drug. Smaller pores may result in slower drug release due to restricted diffusion pathways, while larger pores can enable a faster release. By optimising the porosity, chitosan scaffolds can be engineered to achieve desired therapeutic outcomes, enhancing the efficacy and safety of drug delivery systems.[48,49] Moreover, research by *Pourhaghgouy et al.*[50] on the bioactivity of composite chitosan/BG scaffolds concluded that the incorporation of bioactive glass into the polymeric matrix enhances the scaffold's interaction with bone tissue via the formation of a surface substrate through the apatite layer. Such a substrate enhances bone cell adhesion to the scaffold, and promotes the osteoconductive and osteoproductive properties of the composite.[51–53]

The atomic composition of the resulting composite scaffolds was analysed using energy-dispersive X-ray analysis, as shown in Figs. 2E–2H. EDS mapping confirmed the presence of phosphorus (P), calcium (Ca), and silicon (Si) indicating the presence of BG particles within the chitosan matrix, which was further identified using FTIR and XRD analysis. In samples with lower BG weight fractions (Fig. 2F), visible agglomeration of BG particles was observed. However, as the weight fraction of bioactive glass increased (Figs. 2G and 2H), the agglomeration became less prominent, resulting in a homogeneous dispersion of BG across the polymeric matrix.

3.4 *In vitro* bioactivity

Hydroxyapatite ($Ca_{10}(PO_4)_6(OH)_2$) makes up about 60 % of bone material, and plays a key role in bone tissue repair.[54] Ensuring apatite formation on the surface of the composite scaffold is vital for bone regeneration. *Hench et al.*[55] proposed a mechanism for apatite formation on the BG surface, which begins with an initial reaction of BG with body fluids, resulting in a rapid exchange of alkali or alkaline ions, followed by a pH-assisted hydrolysis of silica groups (Si–O–Si). This is followed by migration of the calcium and phosphate ions from the body into the silica gel layer, accompanied by the nucleation of amorphous calcium phosphates. This nucleation leads to the crystallisation of hydroxyapatite, closely resembling the mineral phase of bone. Over time, the hydroxyapatite layer grows and matures, becoming more crystalline and integrating with the surrounding biological environment. SEM micrographs, (Fig. 3), show the presence of an apatite layer on the surface of the composite scaffolds after 21 days of immersion in SBF. A cauliflower-like apatite formation[50] can be observed on the composite surface. An increase in apatite formations with an increase in BG weight fraction is also discernible. The rate of apatite formation is indicative of the material's bioactive (bone-bonding) potential. It is also important to note that, in this case, the polymeric matrix is not one of these bioactive materials, so the formation of apatite on the composite surface can be directly linked to the presence of BG in the matrix.

XRD analysis of the composite scaffolds after immersion in SBF (Fig. 3E) revealed changes in the surface chemical composition related to the hydroxyapatite mineralisation process. The XRD patterns clearly show the precipitation of hydroxyapatite on the surface of the composite scaffolds after 21 days of SBF incubation, reflected by a sharp diffraction maximum at $2\theta \approx 25.8°$ (002) and 31,7° (211), corresponding to the strongest diffraction maxima of HAp56,57 according to the ICDD hydroxyapatite standard data (ICDD 09-432) (Fig. 3F). Additionally, a small diffraction maximum at $2\theta \approx 31.4°$ and 45.1° was observed, which can be attributed to sodium chloride (NaCl, ICDD1-077-2064), as shown in Fig. 3G. This resulted from incomplete rinsing of the samples after immersion in SBF solution. In conclusion, the addition of BG into the polymeric matrix enhanced the formation of an interactive apatite layer, compared to the pure chitosan scaffold.

3.5 Drug release

The drug release profile of the composite chitosan scaffolds was evaluated in a respective way using a phosphate buffer medium (pH = 7.4) as an in vitro environment. A dynamic release study was conducted to determine the prolonged release of the composite scaffolds. The study spanned a 24-hour period, replacing the medium with a fresh solution at each time point. As shown in Fig. 4, a significant release of DOX was observed during the initial 3-hour period of measurement (time points 1 and 3 h), with cumulative release reaching ≈ 84.31% for DOX25 and ≈ 81.29 % for DOX50. This can be attributed to the hydrogel nature of chitosan, whose structure absorbs and retains water to form a gel-like structure resulting in remarkable swelling and, in this case, release capacity.[58,59] The release rate could be further influenced by doxorubicin's hydrophilic nature and its encapsulation through physical interactions on the surface and within the scaffold itself. These

interactions may also affect the speed at which the drug is released from both the scaffold surface and the matrix.[60] After the burst release, a sustained release phase followed, with ≈ 15.68 % for DOX 25 and ≈ 18.70 % for DOX 50 released over the next 21 h (time points 6, 12 and 24 h). According to *Blaney et al.*[4], DOX has an initial half-life of only about 10 min, followed by a prolonged terminal phase lasting about 24 h. It is recommended that the drug be administered intravenously to ensure fast drug delivery in its most active form. The obtained burst release profile in our case is highly beneficial, as it ensures the rapid delivery of the drug while in its most potent phase, followed by a low concentration slow release, aligning with the recommended administration of the drug.

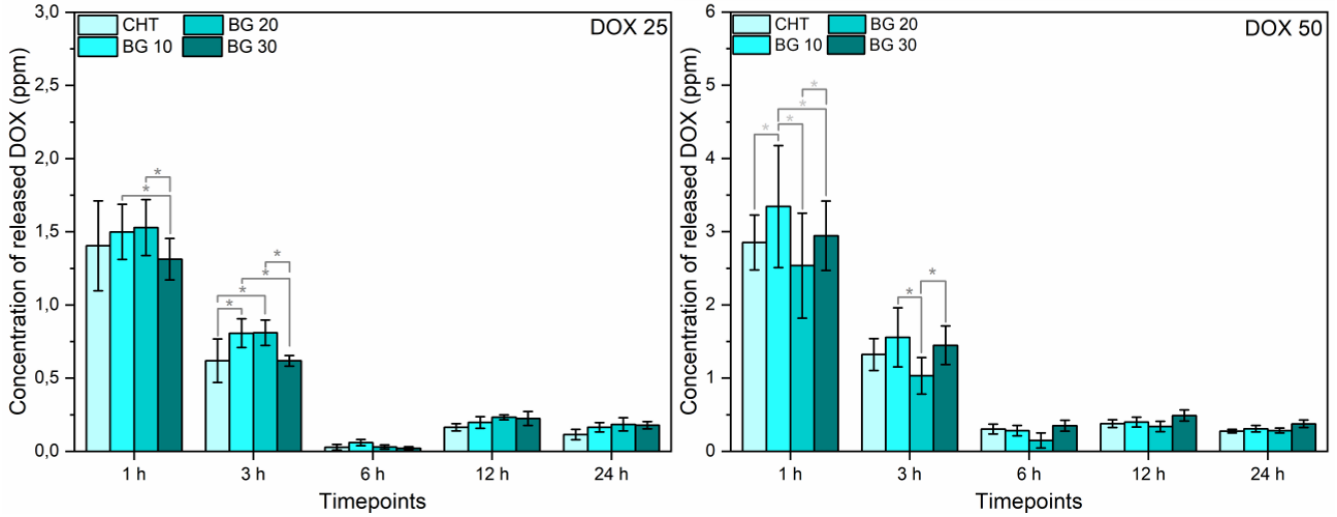

Fig. 4 – Release profile of DOX from composite scaffolds under dynamic conditions (pH = 7.4) over 24 h. The significant difference between the two groups is denoted by an asterisk (*) with $p < 0.05$.

Slika 4 – Otpuštanje DOX-a iz kompozitnih okosnica pri dinamičnim uvjetima (pH = 7,4) tijekom 24 h. Značajna razlika između dviju skupina označena je zvjezdicom (*) s $p < 0,05$.

The incorporation of bioactive glass into the chitosan polymeric matrix resulted in a slight variation in the drug release profile. Specifically, the BG10-DOX25 and BG10-DOX50 samples exhibited the highest release within the first hour, followed by an equalisation in the release profile after three hours across all scaffolds. All scaffolds exhibited an initial burst release (time points 1 and 3 h), followed by a slower, gradual release profile (time points 6, 12 and 24 h). Based on these results, it can be concluded that the incorporation of BG into the polymer matrix had no significant effect on the release profile of DOX from the polymeric matrix, while simultaneously maintaining optimal scaffold porosity and potential osteoinductive and osteoconductive properties of the composite scaffold.

The composite scaffolds showed strong potential for controlled drug release. The initial burst release of DOX ensured a high concentration of the chemotherapeutic agent, potentially achieving immediate therapeutic effects, while the subsequent gradual release sustained drug levels over an extended period, maximising therapeutic efficacy and minimising side effects. These findings indicate the potential of composite chitosan/BG scaffolds as an effective drug delivery system for bone tumour treatment.

4 Conclusion

This study proposes the synthesis of CHT/BG porous composite scaffolds with enhanced bioactivity for use as drug delivery systems. The successful synthesis of bioactive glass through the sol-gel method, and its subsequent incorporation into the chitosan matrix was confirmed through XRD, FTIR, and EDS analysis. SEM micrographs revealed a favourable porous structure with interconnected porosity, supporting cell adhesion and proliferation. The addition of bioactive glass enabled the formation of an interactive apatite layer in biological fluids, enhancing the scaffold's osteoinductive and osteoconductive properties. Furthermore, the addition of BG had no negative effect on drug loading and release, positioning the scaffold as a potential drug delivery system for osteosarcoma treatment and bone tissue regeneration. Further cytotoxicity studies will be conducted to validate the potential of the obtained scaffolds for use in drug delivery and bone tissue regeneration.

ACKNOWLEDGEMENT

This work was supported by the Croatian Science Foundation [grant number UIP-2020-02-6201].

List of abbreviations
Popis kratica

CHT – chitosan

DOX – doxorubicin

TIPS – thermally induced phase separation

BG – bioactive glass

SBF – simulated body fluid

FTIR – Fourier-transform infrared spectroscopy

EDS – energy dispersive X-ray spectroscopy

XRD – X-ray diffraction analysis

SEM – scanning electron microscopy

References
Literatura

1. *S.-Y. Wang, H.-Z. Hu, X.-C. Qing, Z.-C. Zhang, Z.-W. Shao,* Recent advances of drug delivery nanocarriers in osteosarcoma treatment, J. Cancer **11** (2020) 69–82, doi: https://doi.org/10.7150/jca.36588.
2. *E. Pérez-Herrero, A. Fernández-Medarde,* Advanced targeted therapies in cancer: Drug nanocarriers, the future of chemotherapy, Eur. J. Pharm. Biopharm. **93** (2015) 52–79, doi: https://doi.org/10.1016/j.ejpb.2015.03.018.
3. *I. J. Fidler, L. M. Ellis,* Chemotherapeutic drugs – more really is not better, Nat. Med. **6** (2000) 500–502, doi: https://doi.org/10.1038/74969.
4. *S. M. Blaney, M. A. Smith, J. L. Grem,* Doxorubicin: Role in the treatment of osteosarcoma, u G. Bennett Humphrey, H. Schraffordt Koops, W. M. Molenaar, A. Postma (ur.) Osteosarcoma in Adolescents and Young Adults: New Developments and Controversies, Cancer Treat. Res., New York, 1993, str. 55–73.
5. *S. Sritharan, N. Sivalingam,* A comprehensive review on time-tested anticancer drug doxorubicin, Life Sci. **278** (2021) 119527, doi: https://doi.org/10.1016/j.lfs.2021.119527.
6. *M. Kciuk, A. Gielecińska, S. Mujwar, D. Kołat, Ż. Kałuzińska-Kołat, I. Celik, R. Kontek,* Doxorubicin – An Agent with Multiple Mechanisms of Anticancer Activity, Cells **12** (2023) 659, doi: https://doi.org/10.3390/cells12040659.
7. *C. Pérez-Arnaiz, N. Busto, J. M. Leal, B. García,* New Insights into the Mechanism of the DNA/Doxorubicin Interaction, J. Phys. Chem. B **118** (2014) 1288–1295, doi: https://doi.org/10.1021/jp411429g.
8. *C. Carvalho, R. Santos, S. Cardoso, S. Correia, P. Oliveira, M. Santos, P. Moreira,* Doxorubicin: The Good, the Bad and the Ugly Effect, Curr. Med. Chem. **16** (2009) 3267–3285, doi: https://doi.org/10.2174/092986709788803312.
9. *K. Renu, L. P. Pureti, B. Vellingiri, A. Valsala Gopalakrishnan,* Toxic effects and molecular mechanism of doxorubicin on different organs – an update, Toxin Rev. **41** (2022) 650–674, doi: https://doi.org/10.1080/15569543.2021.1912099.
10. *S. Ayla, I. Seckin, G. Tanriverdi, M. Cengiz, M. Eser, B. C. Soner, G. Oktem,* Doxorubicin Induced Nephrotoxicity: Protective Effect of Nicotinamide, Int. J. Cell Biol. **2011** (2011) 1–9, doi: https://doi.org/10.1155/2011/390238.
11. *O. Tacar, P. Sriamornsak, C. R. Dass,* Doxorubicin: An update on anticancer molecular action, toxicity and novel drug delivery systems, J. Pharm. Pharmacol. **65** (2013) 157–170, doi: https://doi.org/10.1111/j.2042-7158.2012.01567.x.
12. *H. Mizutani, S. Tada-Oikawa, Y. Hiraku, M. Kojima, S. Kawanishi,* Mechanism of apoptosis induced by doxorubicin through the generation of hydrogen peroxide, Life Sci. **76** (2005) 1439–1453, doi: https://doi.org/10.1016/j.lfs.2004.05.040.
13. *M. F. Xu, P. L. Tang, Z. M. Qian, M. Ashraf,* Effects by doxorubicin on the myocardium are mediated by oxygen free radicals, Life Sci. **68** (2001) 889–901, doi: https://doi.org/10.1016/S0024-3205(00)00990-5.
14. *A. Choucair, P. Lim Soo, A. Eisenberg,* Active Loading and Tunable Release of Doxorubicin from Block Copolymer Vesicles, Langmuir **21** (2005) 9308–9313, doi: https://doi.org/10.1021/la050710o.
15. *P. Bawa, V. Pillay, Y. E. Choonara, L. C. du Toit,* Stimuli-responsive polymers and their applications in drug delivery, Biomed. Mater. **4** (2009) 022001, doi: https://doi.org/10.1088/1748-6041/4/2/022001.
16. *J. Varshosaz,* The promise of chitosan microspheres in drug delivery systems, Expert Opin. Drug Deliv. **4** (2007) 263–273, doi: https://doi.org/10.1517/17425247.4.3.263.
17. *N. Desai, M. Momin, T. Khan, S. Gharat, R. S. Ningthoujam, A. Omri,* Metallic nanoparticles as drug delivery system for the treatment of cancer, Expert Opin. Drug Deliv. **18** (2021) 1261–1290, doi: https://doi.org/10.1080/17425247.2021.1912008.
18. *V. Chandrakala, V. Aruna, G. Angajala,* Review on metal nanoparticles as nanocarriers: current challenges and perspectives in drug delivery systems, Emergent Mater. **5** (2022) 1593–1615, doi: https://doi.org/10.1007/s42247-021-00335-x.
19. *V. Uskoković, D. P. Uskoković,* Nanosized hydroxyapatite and other calcium phosphates: Chemistry of formation and application as drug and gene delivery agents, J. Biomed. Mater. Res. - Part B Appl. Biomater. **96 B** (2011) 152–191, doi: https://doi.org/10.1002/jbm.b.31746.
20. *M. A. Nazeer, E. Yilgör, I. Yilgör,* Intercalated chitosan/hydroxyapatite nanocomposites: Promising materials for bone tissue engineering applications, Carbohydr. Polym. **175** (2017) 38–46, doi: https://doi.org/10.1016/j.carbpol.2017.07.054.
21. *J. Jagur-Grodzinski,* Polymers for tissue engineering, medical devices, and regenerative medicine Concise general review of recent studies, Polym. Adv. Technol. **17** (2006) 395–418, doi: https://doi.org/10.1002/pat.729.
22. *V. A. Sinani, D. S. Koktysh, B.-G. Yun, R. L. Matts, T. C. Pappas, M. Motamedi, S. N. Thomas, N. A. Kotov,* Collagen Coating Promotes Biocompatibility of Semiconductor Nanoparticles in Stratified LBL Films, Nano Lett. **3** (2003) 1177–1182, doi: https://doi.org/10.1021/nl0255045.

23. *L. Dornjak, M. Kovačić, K. Ostojić, A. Angaits, J. Szpunar, I. Urlić, A. Rogina,* Chitosan-Boric Acid Scaffolds for Doxorubicin Delivery in the Osteosarcoma Treatment, Polymers (Basel). **14** (2022) doi: https://doi.org/10.3390/polym14214753.
24. *M. Farshbaf, S. Davaran, A. Zarebkohan, N. Annabi, A. Akbarzadeh, R. Salehi,* Significant role of cationic polymers in drug delivery systems, Artif. Cells, Nanomedicine Biotechnol. **46** (2018) 1872–1891, doi: https://doi.org/10.1080/21691401.2017.1395344.
25. *K. Prusty, S. K. Swain,* Chitosan-Based Nanobiocomposites for Wound-Healing Applications, u S. K. Swain i M. Jawaid (ur.): Nanostructured Polymer Composites for Biomedical Applications, Biomed. Appl., Elsevier, 2019, str. 295–314.
26. *B. Yang, X. Li, S. Shi, X. Kong, G. Guo, M. Huang, F. Luo, Y. Wei, X. Zhao, Z. Qian,* Preparation and characterization of a novel chitosan scaffold, Carbohydr. Polym. **80** (2010) 860–865, doi: https://doi.org/10.1016/j.carbpol.2009.12.044.
27. *K. Y. Lee, D. J. Mooney,* Hydrogels for Tissue Engineering, Chem. Rev. **101** (2001) 1869–1880, doi: https://doi.org/10.1021/cr000108x.
28. *M. M. Islam, M. Shahruzzaman, S. Biswas, M. Nurus Sakib, T. U. Rashid,* Chitosan based bioactive materials in tissue engineering applications-A review, Bioact. Mater. **5** (2020) 164–183, doi: https://doi.org/10.1016/j.bioactmat.2020.01.012.
29. *R. Sergi, D. Bellucci, V. Cannillo,* A Review of Bioactive Glass/Natural Polymer Composites: State of the Art, Materials (Basel). **13** (2020) 5560, doi: https://doi.org/10.3390/ma13235560.
30. *J. Zhang, J. Nie, Q. Zhang, Y. Li, Z. Wang, Q. Hu,* Preparation and characterization of bionic bone structure chitosan/hydroxyapatite scaffold for bone tissue engineering, J. Biomater. Sci. Polym. Ed. **25** (2014) 61–74, doi: https://doi.org/10.1080/09205063.2013.836950.
31. *N. Reznikov, R. Shahar, S. Weiner,* Bone hierarchical structure in three dimensions, Acta Biomater. **10** (2014) 3815–3826, doi: https://doi.org/10.1016/j.actbio.2014.05.024.
32. *L. L. Hench,* Bioactive Ceramics: Theory and Clinical Applications, u Ö. H. Andersson, A. Yli-Urpo, R.-P. Happonen (ur.), Bioceramics, Elsevier, 1994, str. 3–14.
33. *R. Moonesi Rad, A. Z. Alshemary, Z. Evis, D. Keskin, K. Altunbaş, A. Tezcaner,* Structural and biological assessment of boron doped bioactive glass nanoparticles for dental tissue applications, Ceram. Int. **44** (2018) 9854–9864, doi: https://doi.org/10.1016/j.ceramint.2018.02.230.
34. *T. Kokubo, H. Takadama,* How useful is SBF in predicting in vivo bone bioactivity?, Biomaterials **27** (2006) 2907–2915, doi: https://doi.org/10.1016/j.biomaterials.2006.01.017.
35. *L. Ren, J. Xu, Y. Zhang, J. Zhou, D. Chen, Z. Chang,* Preparation and characterization of porous chitosan microspheres and adsorption performance for hexavalent chromium, Int. J. Biol. Macromol. **135** (2019) 898–906, doi: https://doi.org/10.1016/j.ijbiomac.2019.06.007.
36. *M. P. Klein, C. R. Hackenhaar, A. S. G. Lorenzoni, R. C. Rodrigues, T. M. H. Costa, J. L. Ninow, P. F. Hertz,* Chitosan crosslinked with genipin as support matrix for application in food process: Support characterization and β-d-galactosidase immobilization, Carbohydr. Polym. **137** (2016) 184–190, doi: https://doi.org/10.1016/j.carbpol.2015.10.069.
37. *A. Pawlak, M. Mucha,* Thermogravimetric and FTIR studies of chitosan blends, Thermochim. Acta **396** (2003) 153–166, doi: https://doi.org/10.1016/S0040-6031(02)00523-3.
38. *M. Duarte, M. Ferreira, M. Marvão, J. Rocha,* An optimised method to determine the degree of acetylation of chitin and chitosan by FTIR spectroscopy, Int. J. Biol. Macromol. **31** (2002) 1–8, doi: https://doi.org/10.1016/S0141-8130(02)00039-9.
39. *I. F. Amaral, M. Lamghari, S. R. Sousa, P. Sampaio, M. A. Barbosa,* Rat bone marrow stromal cell osteogenic differentiation and fibronectin adsorption on chitosan membranes: The effect of the degree of acetylation, J. Biomed. Mater. Res. Part A **75A** (2005) 387–397, doi: https://doi.org/10.1002/jbm.a.30436.
40. *N. Mutlu, L. Liverani, F. Kurtuldu, D. Galusek, A. R. Boccaccini,* Zinc improves antibacterial, anti-inflammatory and cell motility activity of chitosan for wound healing applications, Int. J. Biol. Macromol. **213** (2022) 845–857, doi: https://doi.org/10.1016/j.ijbiomac.2022.05.199.
41. *Y.-F. Goh, A. Z. Alshemary, M. Akram, M. R. Abdul Kadir, R. Hussain,* In-vitro characterization of antibacterial bioactive glass containing ceria, Ceram. Int. **40** (2014) 729–737, doi: https://doi.org/10.1016/j.ceramint.2013.06.062.
42. *H. Aguiar, E. L. Solla, J. Serra, P. González, B. León, N. Almeida, S. Cachinho, E. J. C. Davim, R. Correia, J. M. Oliveira, M. H. V. Fernandes,* Orthophosphate nanostructures in SiO_2-P_2O_5-CaO-Na_2O-MgO bioactive glasses, J. Non. Cryst. Solids **354** (2008) 4075–4080, doi: https://doi.org/10.1016/j.jnoncrysol.2008.05.031.
43. *C. O. Correia, Á. J. Leite, J. F. Mano,* Chitosan/bioactive glass nanoparticles scaffolds with shape memory properties, Carbohydr. Polym. **123** (2015) 39–45, doi: https://doi.org/10.1016/j.carbpol.2014.12.076.
44. *X. V. Bui, H. Oudadesse, Y. Le Gal, O. Merdrignac-Conanec, G. Cathelineau,* Bioactivity behaviour of biodegradable material comprising bioactive glass, Korean J. Chem. Eng. **29** (2012) 215–220, doi: https://doi.org/10.1007/s11814-011-0151-0.
45. *H. Pirayesh, J. A. Nychka,* Sol–Gel Synthesis of Bioactive Glass-Ceramic 45S5 and its in vitro Dissolution and Mineralization Behavior, J. Am. Ceram. Soc. **96** (2013) 1643–1650, doi: https://doi.org/10.1111/jace.12190.
46. *J. L. Drury, D. J. Mooney,* Hydrogels for tissue engineering: scaffold design variables and applications, Biomaterials **24** (2003) 4337–4351, doi: https://doi.org/10.1016/S0142-9612(03)00340-5.
47. *I. M. El-Sherbiny, M. H. Yacoub,* Hydrogel scaffolds for tissue engineering: Progress and challenges, Glob. Cardiol. Sci. Pract. **2013** (2013) 38, doi: https://doi.org/10.5339/gcsp.2013.38.
48. *E. Shen, M. J. Kipper, B. Dziadul, M. K. Lim, B. Narasimhan,* Mechanistic relationships between polymer microstructure and drug release kinetics in bioerodible polyanhydrides, J. Control. Release **82** (2002) 115–125, doi: https://doi.org/10.1016/S0168-3659(02)00125-6.
49. *B. Cai, T. Zhong, P. Chen, J. Fu, Y. Jin, Y. Liu, R. Huang, L. Tan,* Preparation, characterization and in vitro release study of drug-loaded sodium carboxy-methylcellulose/chitosan composite sponge, PLoS One **13** (2018) e0206275, doi: https://doi.org/10.1371/journal.pone.0206275.
50. *M. Pourhaghgouy, A. Zamanian, M. Shahrezaee, M. P. Masouleh,* Physicochemical properties and bioactivity of

freeze-cast chitosan nanocomposite scaffolds reinforced with bioactive glass, Mater. Sci. Eng. C **58** (2016) 180–186, doi: https://doi.org/10.1016/j.msec.2015.07.065.
51. *L. L. Hench, R. J. Splinter, W. C. Allen, T. K. Greenlee,* Bonding mechanisms at the interface of ceramic prosthetic materials, J. Biomed. Mater. Res. **5** (1971) 117–141, doi: https://doi.org/10.1002/jbm.820050611.
52. *A. Zamanian, F. Moztarzadeh, S. Kordestani, S. Hesaraki, M. R. Tahriri,* Novel calcium hydroxide/nanohydroxyapatite composites for dental applications: in vitro study, Adv. Appl. Ceram. **109** (2010) 440–444, doi: https://doi.org/10.1179/174367610X12804792635107.
53. *S. Joughehdoust, S. Manafi,* Synthesis and in vitro investigation of sol-gel derived bioglass-58S nanopowders, Mater. Sci. **30** (2012) 45–52, doi: https://doi.org/10.2478/s13536-012-0007-2.
54. *D. S. Gomes, A. M. C. Santos, G. A. Neves, R. R. Menezes,* A brief review on hydroxyapatite production and use in biomedicine, Cerâmica **65** (2019) 282–302, doi: https://doi.org/10.1590/0366-69132019653742706.
55. *C. Y. Kim, A. E. Clark, L. L. Hench,* Early stages of calcium-phosphate layer formation in bioglasses, J. Non. Cryst. Solids **113** (1989) 195–202, doi: https://doi.org/10.1016/0022-3093(89)90011-2.
56. *M. H. Santos, M. de Oliveira, L. P. de F. Souza, H. S. Mansur, W. L. Vasconcelos,* Synthesis control and characterization of hydroxyapatite prepared by wet precipitation process, Mater. Res. **7** (2004) 625–630, doi: https://doi.org/10.1590/S1516-14392004000400017.
57. *I. Mobasherpour, M.S. Heshajin, A. Kazemzadeh, M. Zakeri,* Synthesis of nanocrystalline hydroxyapatite by using precipitation method, J. Alloys Compd. **430** (2007) 330–333, doi: https://doi.org/10.1016/j.jallcom.2006.05.018.
58. *X. Wang, X. Zhen, J. Wang, J. Zhang, W. Wu, X. Jiang,* Doxorubicin delivery to 3D multicellular spheroids and tumors based on boronic acid-rich chitosan nanoparticles, Biomaterials **34** (2013) 4667–4679, doi: https://doi.org/10.1016/j.biomaterials.2013.03.008.
59. *A. Raichur, Thomas, Radhakrishnan, Gnanadhas, D. Chakravortty,* Intracellular delivery of doxorubicin encapsulated in novel pH-responsive chitosan/heparin nanocapsules, Int. J. Nanomedicine **8** (2013) 267, doi: https://doi.org/10.2147/IJN.S37737.
60. *M. L. Tan, P. F. M. Choong, C. R. Dass,* Review: doxorubicin delivery systems based on chitosan for cancer therapy, J. Pharm. Pharmacol. **61** (2009) 131–142, doi: https://doi.org/10.1211/jpp/61.02.0001.

SAŽETAK

Okosnice na temelju kitozana i bioaktivnog stakla kao potencijalni nosači lijeka

*Luka Dornjak** i *Anamarija Rogina*

Suvremeni kemoterapeutski lijekovi nude svestrane i pouzdane načine liječenja različitih oblika sarkoma. Jedan od najšire upotrebljavanih lijekova, doksorubicin, svestran učinak pruža kroz svojstvo interkalacije s DNK, što rezultira brzom razgradnjom DNK i apoptozom stanica raka. Unatoč naprednim svojstvima, njegova primjena rezultira oštećenjem cijeloga tijela dovodeći do kardiotoksičnosti, snižavanja kognitivnih sposobnosti, inhibicije samoobnove i nefropatije. Lokalna i ciljana primjena lijeka uporabom polimernih i kompozitnih materijala jedan je od pristupa za smanjenje nuspojava lijeka. Kitozan, biokompatibilan i biorazgradljiv polimer, može poslužiti kao polimerna matrica za ciljanu dostavu lijeka. Kompozitna okosnica na temelju kitozana i bioaktivnog stakla mogla bi poboljšati ugradnju lijeka i ciljano otpustiti doksorubicin iz kompozitne okosnice, koja ujedno potiče i stvaranje apatitnog sloja poželjnog pri obnovi kosti.

Cilj ovog rada je priprava kompozitnih okosnica kitozan/bioaktivno staklo kao biorazgradljivih nosača doksorubicina pri liječenju tumora kosti. Kompozitne okosnice pripravljene su pri različitim masenim udjelima bioaktivnog stakla (0 – 30 %) unutar polimerne matrice primjenom toplinski inducirane fazne separacije uz naknadnu sublimaciju otapala. Dobivene kompozitne okosnice karakterizirane su rendgenskom difrakcijskom analizom, infracrvenom spektroskopijom s Fourierovom transformacijom i pretražnom elektronskom mikroskopijom potpomognutom energijski razlučujućom rendgenskom spektrometrijom. Lijek je ugrađen uranjanjem pripremljenih okosnica u otopinu doksorubicina različite koncentracije (25 i 50 ppm) tijekom 5 h. Otpuštanje doksorubicina ispitivano je u fosfatnom puferu (pH 7,4) tijekom 24 h fluorescencijskom spektrometrijom.

Ključne riječi

Kitozan, polimer, bioaktivno staklo, doksorubicin, osteosarkom, kompozit

Sveučilište u Zagrebu Fakultet kemijskog inženjerstva i tehnologije,
Trg Marka Marulića 19, 10 000 Zagreb

Izvorni znanstveni rad
Prispjelo 28. lipnja 2024.
Prihvaćeno 2. rujna 2024.